J. Fluid Mech. (2000), *vol.* 416, *pp.* 217–237. Printed in the United Kingdom

The normal field instability in ferrofluids: hexagon–square transition mechanism and wavenumber selection

By BÉRENGÈRE ABOU[1]†, JOSÉ-EDUARDO WESFREID[1] AND STÉPHANE ROUX[2]

[1] Laboratoire de Physique et Mécanique des Milieux Hétérogènes (PMMH), UMR CNRS 7636, Ecole Supérieure de Physique et Chimie Industrielles de Paris (ESPCI), 10 rue Vauquelin, 75231 Paris Cedex 05, France

[2] Laboratoire "Surface du Verre et Interfaces", UMR CNRS 125, 39 quai Lucien Lefranc, 93303 Aubervilliers Cedex, France

(Received 13 January 1999 and in revised form 13 March 2000)

When a ferrofluid layer is subjected to a uniform and vertically oriented magnetic field, an interfacial instability occurs, above a critical value of the magnetic field, giving rise to a hexagonal array of peaks. On increasing the magnetic field, a smooth morphological transition from the hexagonal array to a square array was observed above a second threshold. The hexagon–square transition phenomenology, in addition to the role of penta–hepta defects initially present in the hexagonal pattern, was investigated. Furthermore, the pattern and wavenumber selection was studied by two different procedures: first by imposing jumps in field intensity and second by varying the magnetic field in a quasi-static way. The results obtained were very different for the two procedures. They indicated that the square pattern was a metastable state induced by the compression of the hexagonal pattern on increasing the control parameter. This hypothesis was confirmed by performing an additional experiment where the pattern was isotropically compressed. In this experiment, the transition was induced at a constant magnetic field lower than the transition onset value. However, the theoretical values for stability domains of hexagons and squares proposed in the literature were found to not agree with the experimental values.

1. Introduction

Ferrofluids are colloidal suspensions of small monodomain magnetic particles with an average size of 100 Å in a non-magnetic carrier fluid. When a ferrofluid layer is subjected to a uniform and vertically oriented magnetic field, an interfacial instability occurs, above a critical value of the magnetic field, giving rise to a hexagonal array (pattern) of peaks. The instability mechanism is described thus: in the presence of a vertical magnetic field, the perturbations of the ferrofluid surface concentrate the magnetic flux. The resulting magnetic force tends to drive the perturbation further, while surface tension and gravitational forces have a stabilizing influence. When the magnetic force exceeds the stabilizing forces, an instability develops. The stability analysis, for an infinite and non-viscous ferrofluid layer in vacuum, was carried out

† Present address: Laboratoire de Physique Statistique, UMR CNRS 8550, Ecole Normale Supérieure, 24 rue Lhomond, 75231 Paris Cedex 05, France.

by Cowley & Rosensweig in 1967. The critical value of the magnetic field for the onset of the instability H_{crit}, and the critical wavenumber k_{crit} (or critical wavelength $\lambda_{crit} = 2\pi/k_{crit}$) are derived from this analysis:

$$k_{crit} = (\rho g/\gamma)^{1/2} = k_c,$$

$$H_{crit} = \left(\frac{2}{\mu_0}\frac{(\mu_0/\mu + 1)}{(\mu_0/\mu - 1)^2}\right)^{1/2} (\rho g \gamma)^{1/4},$$

where ρ is the fluid density, γ the surface tension, μ the magnetic permeability, g the acceleration due to gravity and k_c the capillary wavenumber. In a typical experiment, the critical wavelength (which equals the capillary wavelength) is of the order of 1 cm and the critical magnetic field of the order of $10^4\,\mathrm{A\,m^{-1}}$. Since the work of Cowley & Rosensweig, the linear stability analysis has been explored further, including the influence of viscosity and finite thickness of the ferrofluid layer (Zelazo & Melcher 1969; Brancher 1980; Salin 1993; Abou, Néron de Surgy & Wesfreid 1997†).

On increasing the magnetic field, the hexagonal pattern changes to a square pattern above a second threshold. In 1970, the existence of a stationary square pattern for higher values of magnetic field was predicted by Gailitis (1977), using an energy-variational method. This result was also obtained by the mathematical bifurcation analysis of Twombly & Thomas (1980). At this time, the hexagon–square transition had only been partially observed in one test of Cowley & Rosensweig's experiment. Later, in 1985, it was also confirmed in experiments (Allais & Wesfreid 1985) and numerical simulations (Boudouvis *et al.* 1987).

The competition between hexagons and squares can be thought of in the more general context of transitions between patterns from higher to lower symmetry. This has been theoretically analysed by means of an energy minimization principle (Gailitis 1977; Kuznetsov & Spektor 1976) or symmetry considerations (Silber & Knobloch 1988), and also in the framework of the generalized Swift–Hohenberg equation (Herrero, Pérez-Garcìa & Bestehorn 1994; Kubstrup, Herrero & Pérez-Garcìa 1996). This competition has also been recently observed in Bénard–Marangoni convection (Nitschke-Eckert & Thess 1995; Schatz *et al.* 1999) and in shaken granular media by Melo, Umbanhowar & Swinney (1995). A number of numerical simulations that take into account the competition between hexagons and squares in various systems have been performed (Herrero *et al.* 1994; Nitschke-Eckert & Thess 1995; Kubstrup *et al.* 1996; Bestehorn 1996; Bragard & Velarde 1998).

In the present paper, we experimentally study the hexagon–square transition occurring in a ferrofluid. Section 2 describes the experimental design and § 3 presents the structures of the hexagonal and square patterns, as well as their topological defects, as revealed by means of a two-dimensional FFT method. In § 4, we describe the hexagon–square transition phenomenology. The hexagon–square transition involves a change in the wavenumber at the onset of transition and the formation of fronts, in which the perpendicular hexagonal pattern wavevector is conserved. Penta–hepta defects contained in the hexagonal pattern constitute nucleation sites for the transition. In the next section, the wavenumber selection following jumps in control parameter and when increasing and decreasing the control parameter in a quasi-static way is presented and discussed, together with hysteresis and stability. We conclude that the

† Note that equation (1) in this article, where the critical magnetic field is defined $\left(H_{crit} = \left(\frac{2}{\mu_0}\frac{(\mu_0/\mu + 1)}{(\mu_0/\mu - 1)^2}\right)^{1/2} (\rho g \gamma)^{1/4}\right)$ contains a misprint.

FIGURE 1. Penta–hepta defects represented by pairs of white and grey dots. The hexagonal pattern contains lines of defects that form grain boundaries. Several hexagonal patterns with different orientations in the container are observed.

hexagonal pattern at k_{crit} and the square pattern above the onset of instability are metastable states of the system. In the final § 6, an additional experiment performed in a hopper shows that the transition to the square pattern can be induced by isotropically compressing the hexagonal pattern, at constant magnetic field lower than the transition threshold.

2. The experimental design

The experimental design consisted of a cell with a pool of ferrofluid in a uniform, vertically oriented magnetic field produced by coils ($D = 80$ cm in diameter) arranged as a Helmholtz pair, with a water cooling system. A video CCD camera positioned above the upper coil recorded images of the ferrofluid surface. The camera captured by reflection any local flat area on the surface (Rosensweig 1985). Digital image acquisition and analysis were performed by means of the public domain NIH-Image software.† This programme allowed us to compute a two-dimensional Fourier transform of the grey level intensity of the images for pattern characterization, defect identification and localization.

Experiments were conducted in hexagonal, cylindrical or square containers. In the cylindrical container (16.9 cm in diameter), the hexagonal pattern was found to have many defects, consisting of pentagonal–heptagonal pairs of peaks, called penta–hepta defects (figure 1). In most cases, the defects tended to form grain boundaries separating domains with different orientations. In order to decrease the number of defects, we performed experiments in a hexagonal-shaped container with Plexiglas walls and a side length equal to $b = 14$ cm. The side length was selected on the basis of a preliminary investigation: at the onset, the hexagonal pattern appeared with a wavelength λ equal to the capillary wavelength λ_c, which did not change when increasing the magnetic field (§ 5). The hexagonal pattern wavenumber is related to

† Developed at the US National Institutes of Health and available on the Internet at http://rsb.info.nih.gov/nih-image/.

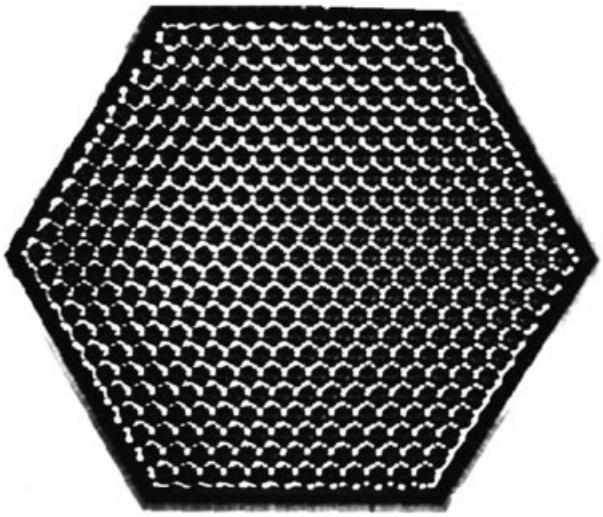

FIGURE 2. Hexagonal pattern without any penta–hepta defects; there are about 400 peaks in the hexagonal container.

the distance between peaks d by $\lambda = \sqrt{3}/2\,d$. The side length was chosen to be an integer number of the critical distance between peaks ($b \simeq 11 d_{crit}$). However, the presence of a meniscus at the lateral walls (which became higher and larger with increasing magnetic field) as well as the variation of the ferrofluid surface tension as a function of temperature made this adjustment approximate. When the side length was not exactly an integer number of the critical distance between peaks, the maximum strain of the pattern equalled $0.5/11 \simeq 5\%$ in the container and the elasticity of the hexagonal pattern was sufficient for a defect-free structure to occur (figure 2). Once the instability set in, there were about 400 peaks in the hexagonal container. The different containers were filled to a depth of $a = 1.3$ cm, which can be considered as an infinite depth in terms of magneto-hydrodynamic behaviour (Abou *et al.* 1997).

The magnetic field, measured with a Hall effect Gaussmeter, at the level of the liquid surface but with an empty container, was uniform to 4% over the hexagonal container. In the presence of the fluid, the most severe inhomogeneity of the magnetic field was expected at the edge of the container where the unavoidable presence of the meniscus masked its effect. A maximum value of the magnetic field of approximately $28000\,\mathrm{A\,m^{-1}}$ was obtained. The drift of the magnetic field in these experiments was within the sensitivity of the Hall probe used, which was less than 3% of the field range. Hence, hereafter it will be neglected.

Experiments were performed with the ferrofluid APG 512 A, synthetized by *Ferrofluidics Corporation*. It was prepared by grinding 3–8% magnetite by volume in a synthetic esther to which 18–30% by volume of an oil-soluble dispersant and 1–2% by volume of an aromatic amine were added. The values of physical parameters of the magnetic fluid APG 512 A (density ρ, saturation magnetization M_{sat}, initial relative magnetic permeability μ_r and dynamic viscosity η), except surface tension γ, were given by *Ferrofluidics Corporation* (table 1). The surface tension was measured with a digital tensiometer KRÜSS (type K10 ST), by means of the Whilhelmy method at ambient temperature $T = 293$ K.

Ferrofluid	ρ (kg m^{-3})	η (N m^{-2} s)	μ_r	M_{sat} (A m^{-1})	γ (N m^{-1})
APG 512 A	1260	0.075	2.4	23810	0.028 ± 0.002

TABLE 1. Ferrofluid APG 512 A parameters.

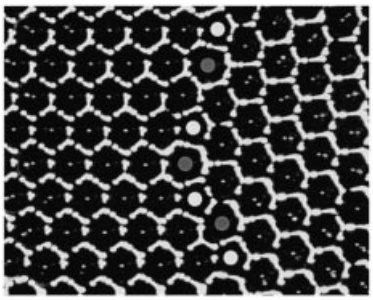

FIGURE 3. Penta–hepta defects close to each other form a grain boundary in the hexagonal pattern: two hexagonal patterns with different orientations are observed.

3. The hexagonal and square patterns

The structures of the hexagonal and square patterns, as well as their respective defects, found in the experiments are shown. The patterns were studied by means of a two-dimensional Fourier-transform $F(\boldsymbol{k})$ of the grey level of the images (FFT), following previous studies in a Rayleigh–Bénard system (Ciliberto, Pampaloni & Pérez-Garcìa 1991). The FFT method provided the modulus $\tilde{F}(\boldsymbol{k})$ in Fourier space. For a hexagonal pattern, $\tilde{F}(\boldsymbol{k})$ consists of three pairs of peaks $(\boldsymbol{k}_i, -\boldsymbol{k}_i)$, $i = (1, 2, 3)$ at 120° with respect to each other and their harmonics. In the analysis, all but one pair of peaks are filtered out at the fundamental modes $\boldsymbol{k}$ and $-\boldsymbol{k}$ on $F(\boldsymbol{k})$ and an inverse transform is performed: one straight-line pattern is then reconstructed. The hexagonal pattern can be viewed as the linear superposition of three modes at 120° with respect to one another, each mode contributing a pair of peaks. The picture grey level is not a direct measurement of the amplitude of the surface deformation however; digital image analysis allows us to obtain the values of $|\boldsymbol{k}_j|$ but not the values of the amplitudes of these Fourier modes.

As mentioned earlier, the hexagonal pattern is not regular in practice and contains defects. They have been studied mainly in Bénard–Marangoni instability conditions (Pantaloni & Cerisier 1983). Boundary conditions that are incompatible with the formation of a regular pattern can force the structures to develop defects. In the case of a pattern with a penta–hepta defect, the FFT method shows that the core of the defect corresponds to two dislocations in the hexagonal pattern. Two out of the three directions of the hexagonal pattern are altered by these dislocations. At the core of the defect, only one straight-line pattern out of the three survives this translocation (Ciliberto *et al.* 1990; Abou 1998).

When several penta–hepta pairs are close to each other in the hexagonal pattern, they form lines of defects called grain boundaries (figure 3). While a single defect only locally alters the hexagonal pattern, a line of such defects separates the medium into two hexagonal patterns with different orientations. Above the threshold of instability, the hexagonal pattern appears with a configuration and number of defects that depends on its formation process. The whole structure undergoes a slow time

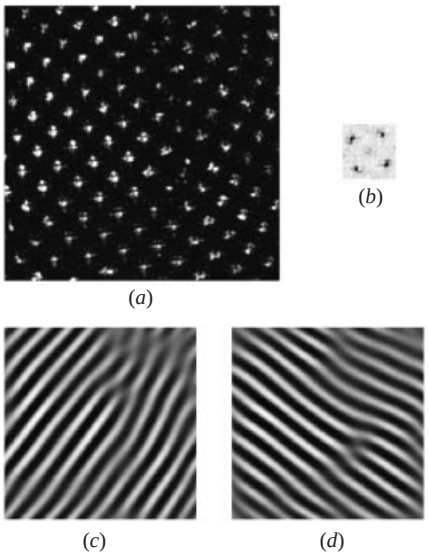

FIGURE 4. Dislocations in the square pattern: (*a*) image of the square pattern; (*b*) power spectrum of the grey level image – this figure also shows the fundamental modes; (*c*, *d*) the two fundamental modes of (*a*) at 90° with respect to each other as produced by the Fourier filtering.

relaxation over a period of a few hours during which the various defects present in the structure can move or disappear while the magnetic field remains constant and uniform.

On increasing the magnetic field above the value for the formation of the hexagonal pattern, the peaks move to form a square lattice, above a second threshold. A Fourier analysis of the image of a square pattern shows that it can be viewed as the linear superposition of two modes at 90° with respect to each other. When the boundary conditions (cylindrical and hexagonal containers) are incompatible with the formation of a square pattern without any defects, either isolated dislocations (figure 4) or a grain boundary produced by the junction of two sets of squares with different orientations (figure 5) occur.

4. Transition between hexagonal and square patterns

4.1. *The phenomenology of the hexagon–square transition*

On progressively increasing the magnetic field, the hexagonal pattern formed at the threshold of instability initially remains exactly the same. The peak height increases, but no change in their number is observed and there is no variation in the location or number of penta–hepta defects. Thus, the hexagonal pattern wavenumber – equal to the capillary wavenumber k_c – remains constant. Upon further increase of the magnetic field, a smooth morphological transition to the square pattern, above a certain value of the magnetic field was observed. The peaks of the ferrofluid in the container move and rearrange from a triangular symmetry into a square symmetry. This defines a second transition characterized by a well-defined value of the magnetic field. When penta–hepta defects are present, the square cells clearly nucleate at the defects.

The geometrical mechanism of the transition in ferrofluids, when there are no defects in the hexagonal pattern can be demonstrated. An experiment was performed

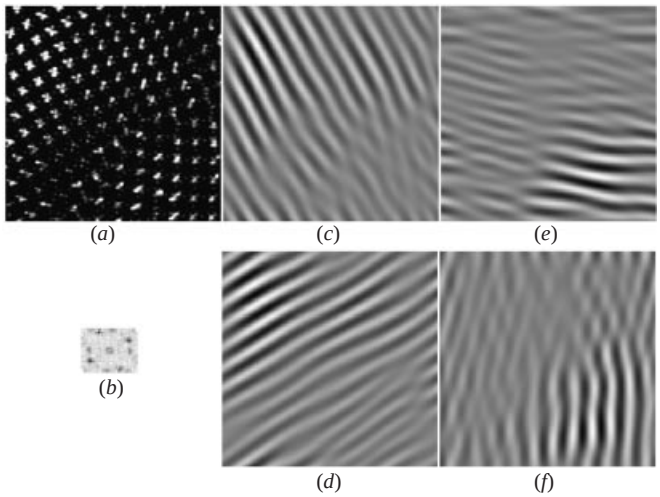

FIGURE 5. A typical defect of the square pattern: (*a*) a grain boundary which is the junction of two square patterns with different orientations; (*b*) power spectrum of the grey level image; the two pairs of modes involved (*c*, *d*) and (*e*, *f*) are shown.

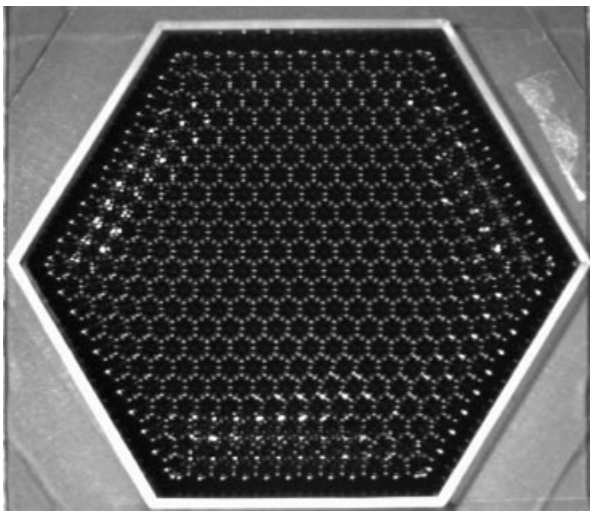

FIGURE 6. Hexagonal pattern without any defects: the transition begins at the lateral walls. Stable fronts between the coexisting symmetries are observed.

in a hexagonal container where a defect-free hexagonal pattern was established. A transition first begins along the lateral walls as shown in figure 6, or along the diagonal of the container. The hexagon–square transition begins as follows: single or multiple rows of peaks in the container propagate along their orientation axis (Ox_1 as shown in figure 7). This propagation locally transforms the triangular symmetry into a *transient rectangular symmetry*, which can be regarded as a strained square symmetry. Upon further increase of the magnetic field, this rectangular symmetry changes into a square symmetry by expanding in the perpendicular direction Ox_4 (as shown in figure 7). After the onset of the transition, stable fronts between the coexisting symmetries within a certain range of the control parameter are observed.

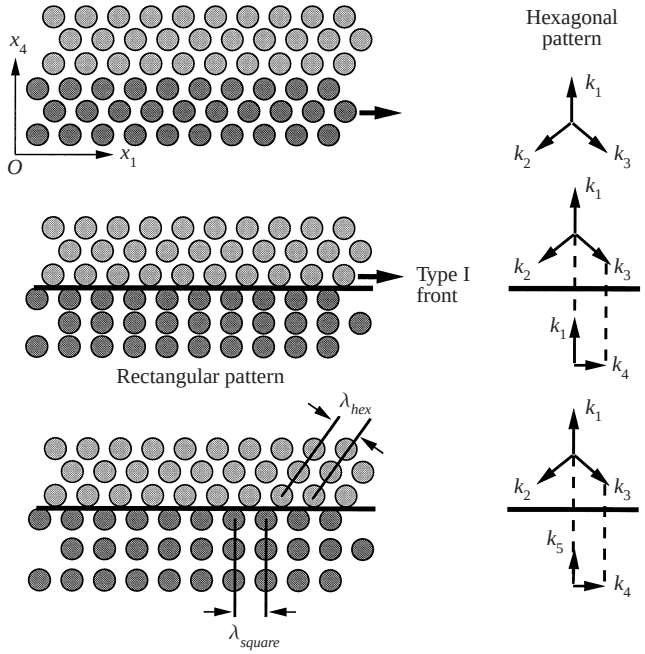

FIGURE 7. The hexagon–square transition begins when one row of peaks slides with respect to its neighbours; this locally involves the formation of a transient rectangular symmetry, which relaxes into a square symmetry on the further increase of the magnetic field. On the right of the figure, the Fourier modes of the patterns are represented. Note that $k_4 = \sqrt{3}/2\,k_1$ and $k_4 = k_5$.

Figure 7 shows a schematic of the transition phenomenology. The translational motion of the rows of peaks involves the formation of a strained square symmetry. This strained square symmetry relaxes into the square symmetry by decreasing $|\boldsymbol{k}_1|$ upon further increases of the magnetic field. This transition phenomenology results in the formation of the so-called type I fronts between hexagons and squares, which means that the wavevector perpendicular to the front is conserved. This experimental result confirms the numerical simulations of the generalized Swift–Hohenberg model equation, where a pinned type I front between the two symmetries is observable for a full range of the control parameter (Kubstrup *et al.* 1996). Another type of front (type II) for which the wavevector parallel to the front is conserved, is shown to be unstable in this Swift–Hohenberg model. This finding is in good agreement with our experimental observations.

The transition, occurring at a fixed number of peaks, involves a change in wavenumber in the system (figure 7). For the hexagonal pattern, the wavenumber is $k_{hex} = 2\pi/\lambda = 4\pi/\sqrt{3}d$ and for the square pattern it is $k_{square} = 2\pi/\lambda = 2\pi/d$, where d is the distance between peaks. Near the onset, the two symmetries coexist with different wavenumbers:

$$k_{square} = \sqrt{3}/2\,k_{hex}.$$

The significant findings in this experimental result were not taken into account in the theoretical analysis of Gailitis and in numerical simulations where the patterns wavenumbers are taken to be equal to the critical one (Gailitis 1977; Herrero *et al.* 1994; Kubstrup *et al.* 1996). Section 5 explains the significance of how these wavenumbers evolve on the further increase of magnetic field.

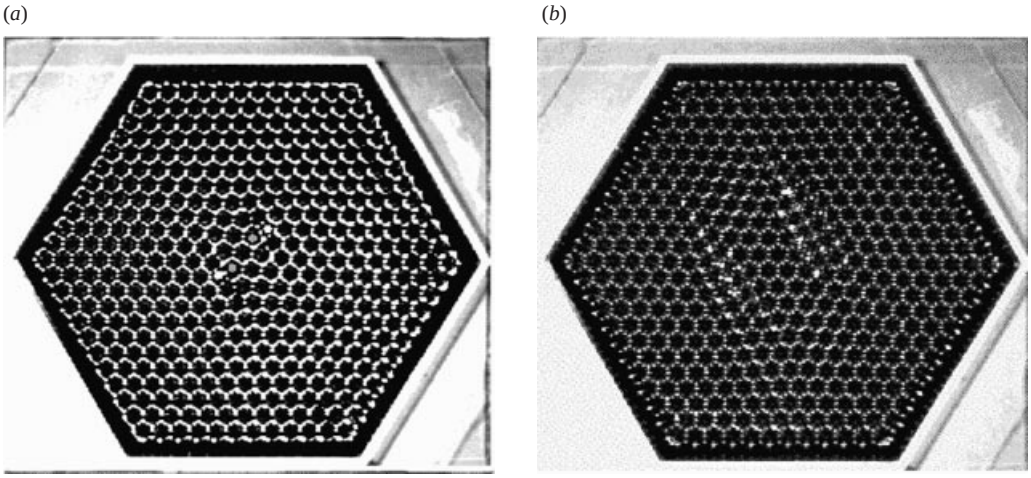

FIGURE 8. The hexagon–square transition begins with the penta–hepta defects. The magnetic field is increased in a quasi-static way. (*a*) $H_{crit} < H < H_{hs}$; (*b*) $H = 1.06\ H_{hs}$, where H_{crit} is the critical magnetic field and H_{hs} the hexagon–square transition threshold. Pinned type I fronts are clearly observable between the two symmetries.

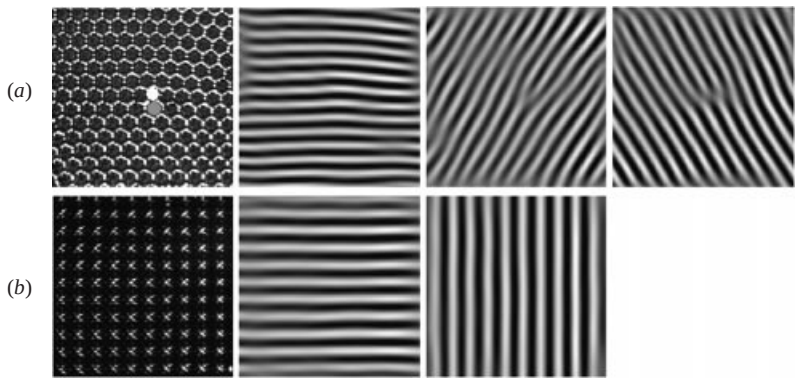

FIGURE 9. (*a*) the hexagonal pattern with a penta–hepta defect and its three modes obtained from Fourier filtering the initial image; (*b*) the square pattern formed from the hexagonal pattern in (*a*) by increasing the magnetic field, and its two modes reconstructed from Fourier filtering. The non-altered mode of the penta–hepta defect is conserved during the transition.

4.2. *Role of the penta–hepta defects in the transition*

Experimentally, the penta–hepta defects act as nucleation centres which trigger the transition from the hexagonal to the square pattern as shown in figure 8. On increasing the magnetic field, the transition clearly begins at the penta–hepta defect. In our measurements, we find that the hexagon–square transition occurs for a lower magnetic field when penta–hepta defects are present and in § 5 give quantitative values of the transition thresholds. In figure 9(*a*) (left-hand image), the scenario of the transition starting at a penta–hepta defect can be seen clearly. The Fourier modes are shown on the right-hand-side images in this figure. The translational motion of the rows of peaks begins first at the penta–hepta defect and then proceeds along the direction of the mode which is not altered by a dislocation (horizontal direction shown in (*a*), second image). Most importantly, only the peaks near the defect move. On increasing

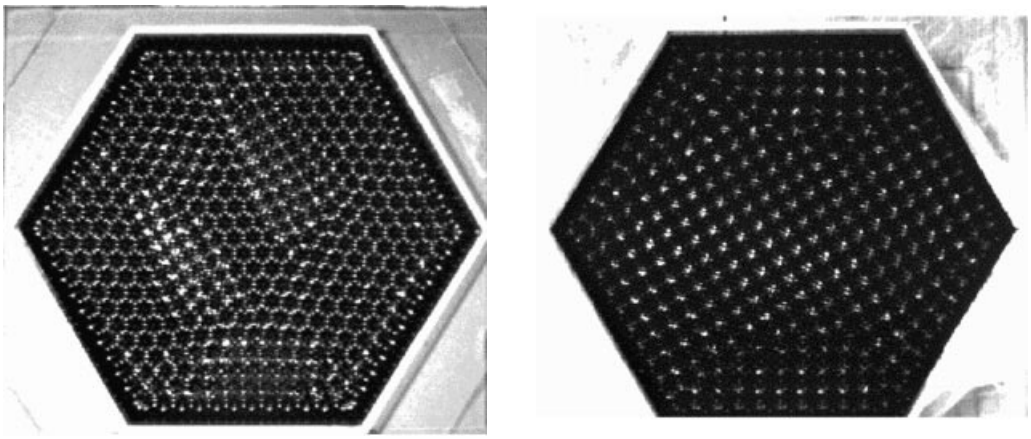

FIGURE 10. Grain boundaries in the square pattern; the magnetic field is increased continuously from $H = 1.1\ H_{hs}$ to $H = 1.6\ H_{hs} \simeq M_{sat}$.

the magnetic field, this motion propagates into the entire row of peaks. The surviving mode of the hexagonal pattern at the core of the defect then becomes one of the two modes of the square pattern, as can be seen in figure 9(*b*).

The characteristics of the square phase are present in the core of the penta–hepta defect (Ribotta & Joets 1983; Coullet, Emilson & Plaza 1991; Ciliberto *et al.* 1991). Based upon a penta–hepta defect, we can predict how the square pattern will develop at the core of the defect.

On the further increase of the magnetic field, the square pattern slowly invades the hexagonal pattern. This invasion occurs from different places in the container: primarily from the penta–hepta defects and then from the lateral walls. This results in the formation of various square patterns with different orientations, separated by grain boundaries as shown in figure 10. On increasing the magnetic field, the coalescence of peaks at square-pattern grain boundaries is observed with the consequence that the square-pattern wavenumber decreases. The amount of coalescence increases with the magnetic field and reaches a saturation value. Indeed, when the ferrofluid magnetization M reaches a value close to saturation, further increase of the magnetic field has no effect. Approximately 30% of peaks may disappear by coalescence. When decreasing the magnetic field, the hexagonal pattern invades and ejects the square pattern from grain boundaries. The grain boundary is replaced by two type I fronts with the transition being hysteretic. The following section addresses this point in a quasi-static way.

5. The wavenumber selection

The wavenumber was selected by varying the magnetic field in a quasi-static way and also by using jumps in field intensity. The wavenumber selection is thus shown to depend on the process used. Linear stability analysis predicts that this system behaves as a semi-infinite and inertial ferrofluid layer, which means that thickness and viscosity effects can be neglected (Abou *et al.* 1997). Findings can be presented in the form of corresponding results:

$$k_{crit} = k_c = (\rho g/\gamma)^{1/2},$$

$$H_{crit} = \left(\frac{2}{\mu_0} \frac{(\mu_0/\mu + 1)}{(\mu_0/\mu - 1)^2} \right)^{1/2} (\rho g \gamma)^{1/4},$$

$$k_m/k_{crit} = \tfrac{1}{3}[2(\varepsilon + 1) + (4(\varepsilon + 1)^2 - 3)^{1/2}],$$

where k_m is the wavenumber of maximum growth rate. The control parameter ε is a measure of how far the system is from criticality, when H is the applied magnetic field:

$$\varepsilon = H^2/H_{crit}^2 - 1$$

The measured critical magnetic field and wavenumber are respectively $H_{crit} = 11100 \pm 800\,\mathrm{A\,m^{-1}}$ and $k_{crit} = 645 \pm 30\,\mathrm{m^{-1}}$. These experimental values are in good agreement with linear theory predictions of $H_{crit} = 11750\,\mathrm{A\,m^{-1}}$ and $k_{crit} = 664\,\mathrm{m^{-1}}$. When the hexagonal pattern at k_{crit} is established in the hexagonal container, the number of peaks in the hexagonal container is about $N_{crit} = 400$.

Unless otherwise stated, the error in the measurement of k/k_{crit} is of order 2% in the hexagonal pattern and of order 5% in the square pattern. This error is due to the presence of grain boundaries in the square pattern, unavoidable due to the hexagonal shape of the container. Moreover, the error in the applied magnetic field H is of the order of 3% and corresponds to the systematic error in the field measurement with the Gaussmeter.

5.1. *Using jumps in field intensity*

The experimental procedure was as follows: the vigorously agitated container was rapidly introduced into the magnetic field, which destroys any pattern formed during this step. The system was then allowed to reach an equilibrium state. For any $H > H_{crit}$, a hexagonal array of peaks is always favoured. The larger the magnetic field, the smaller the hexagonal pattern wavenumber, denoted k^*, where $k^* < k_{crit}$. These reproducible results are shown in figure 11 (represented by the symbol $*$). The marginal stability curve, deduced by the linear theory analysis for a semi-infinite and inertial ferrofluid layer, is shown as a dashed curve. The wavenumber selected decreases down to $0.72k_{crit}$ when the maximum value of magnetic field $\varepsilon_{max} = 3.6$ (when $H \simeq M_{sat}$). This corresponds to the number of peaks in the container equal to $0.5N_{crit}$. As the growth rate tends to zero at the onset of instability, the corresponding equilibrium state is not obtained experimentally. However, extrapolation of our data suggests that $\varepsilon \to 0$ is compatible with $k \to k_{crit}$, although with a very steep variation $|\partial(k/k_{crit})/\partial\varepsilon| \gg 1$.

The time needed for the structure to reach a stationary hexagonal pattern varies as a function of the imposed magnetic field. When $\varepsilon \lesssim 1$, the hexagonal pattern forms rapidly in the container, in a time of the order of a few seconds. When ε increases in value, we first observe a transient structure of coexisting square and triangular symmetries and the equilibrium structure forms in a few minutes. The experimental procedure (agitating the container) could influence the wavenumber selection. Nevertheless, the experimental results turn out to be very convincing. They are reproducible despite the variable nature of the experimental conditions.

In some experiments, performed in thin layers, the wavenumber of maximum growth rate k_m is shown to be selected when using jumps in field intensity (Bacri, Perzynski & Salin 1988; Valet & Wesfreid 1988). In these experiments, the pattern forms over a time larger than required to establish the magnetic field.

In our experiments, the wavenumber of maximum growth rate, predicted by linear theory analysis (and shown in figure 11), is not selected and the wavenumber selection

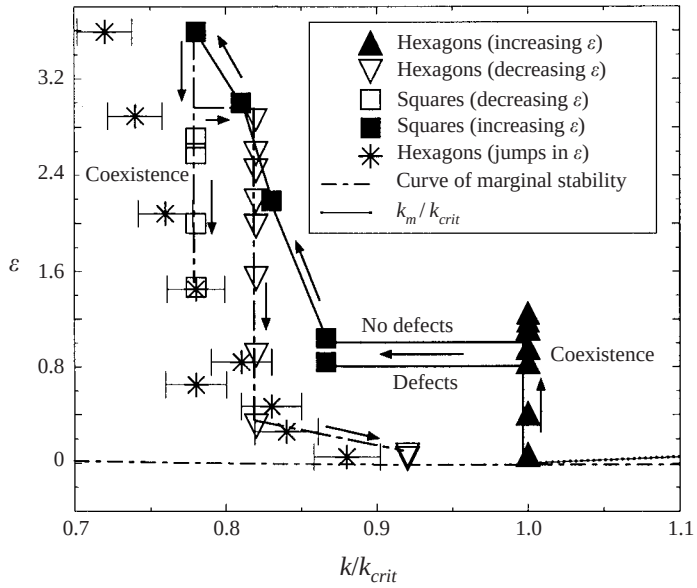

FIGURE 11. Wavenumber selection by two procedures: jumps in field intensity and quasi-static variation of magnetic field. The wavenumber of maximum growth rate k_m and the marginal stability, deduced from linear theory analysis, are also indicated.

is not linear (Wesfreid & Zaleski 1983). The results on wavelength selection obtained by this method of descending steps cannot give full information on the nonlinear domain of stability (Busse balloon of this instability). However, we can expect that the low-k branch of this domain is accessible in this experiment. In addition to the non-uniformity in the magnetic field around the cell walls, this change occurs over very short distances and does not allow the imposition of the wavelength selection mechanism, which occurs in systems with ramp changes of ε. In addition, where large deformations of the interface were observed, the theoretical hypotheses of the linear stability analysis break down.

5.2. *Varying the magnetic field in a quasi-static way*

The wavenumber selection, when increasing and decreasing ε in a quasi-static way, is also shown in figure 11. The experiment is performed in the hexagonal container where a hexagonal pattern with a few isolated penta–hepta defects has been established. During the experiments, the magnetic field was continuously and slowly increased or decreased and then sufficient time allowed for the system to reach a steady state. The time needed for the pattern to reach a steady state was of the order of a few seconds.

Starting from an initially flat interface, the magnetic field was increased continuously until a hexagonal pattern developed. Its wavenumber corresponds to $k_{crit} = k_c$ and remains a constant as ε (▲) increases, until the pattern disappears completely, and is replaced by the square pattern. The hexagon–square transition occurs with $\varepsilon_{hs} = 0.84 \pm 0.17$ for a hexagonal pattern with penta–hepta defects, or at $\varepsilon_{hs} = 1.04 \pm 0.17$ for a hexagonal pattern without any defects, where ε_{hs} is the non-dimensioned transition threshold. As seen previously and as shown in figure 11, at the onset of transition there is an abrupt change in wavenumber.

Above the onset, the two symmetries, triangular and square, coexist in the range $0.84 \leqslant \varepsilon \leqslant 1.25$ with different wavenumbers and separated by pinned type I fronts (see

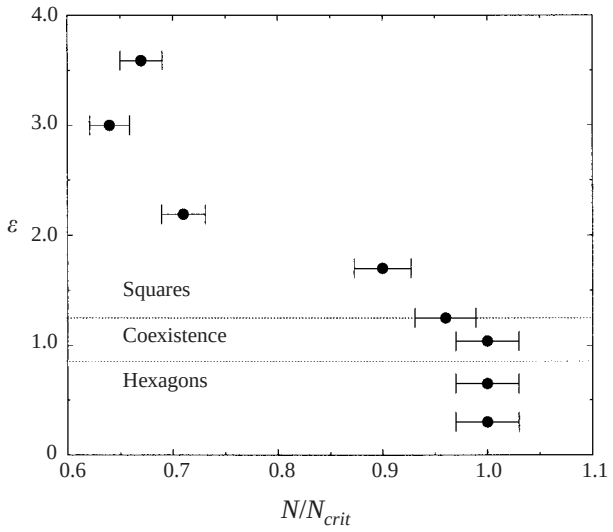

FIGURE 12. Number of peaks in the container as a function of increasing magnetic field.

§ 4). On increasing ε, the square pattern appears in the container with its wavenumber decreasing with increasing ε (■) (while the wavenumber of the hexagonal pattern remains constant and equal to k_{crit}(▲)). The spatial extension of the square pattern is accompanied by the coalescence of peaks at the grain boundaries. The first peak coalescence occurs above the onset at $\varepsilon = 1.04 \pm 0.17$. The proportion of peak coalescences reaches its maximum value when $H_{max} \simeq M_{sat}$, where about a third of the 400 peaks have disappeared. Figure 12 shows the dependence of the number of peaks N/N_{crit} on ε, when ε is increased in a quasi-static way.

On decreasing ε from $\varepsilon_{max} = 3.6$, a smooth and hysteretic transition to the hexagonal pattern is observed. The hexagonal pattern starts to replace the square pattern at $\varepsilon_{sh} = 2.86 \pm 0.21$ and has totally replaced it at $\varepsilon = 1.47 \pm 0.18$. There is coexistence of the two symmetries, separated by type I fronts, in the range $1.47 \leqslant \varepsilon \leqslant 2.86$. The hexagonal pattern wavenumber is equal to $0.82k_{crit}$ in this instance because the coalescence occurs when increasing ε. On decreasing ε, the wavenumber of the hexagonal pattern remains constant (▽, figure 11) until the creation of new peaks in the range $0.31 \geqslant \varepsilon \geqslant 0.07$ is observed. The resulting hexagonal-pattern wavenumber increases up to $0.92k_{crit}$, which corresponds to 90% of the initial number of peaks in the container. The scenario of peak creation is as follows: the new peak always grows with a penta–hepta defect. By a rearrangement of the neighbouring peaks, the new peak becomes the centre of the pentagon of a new defect. This process can be seen as a displacement of the original defect along one of the two altered directions of the hexagonal pattern, at the original penta–hepta defect (figure 13). The two altered directions seem equivalent. The new defect is then the nucleation site of another new peak. The whole process of creation is relatively rapid and results in the expulsion of the defects from the bulk of the body at the lateral walls.

The cycle shown in figure 11 was performed by increasing the magnetic field until its maximum value $\varepsilon_{max} = 3.6$. If the value of ε_{max} is changed, the hexagonal-pattern wavenumber on decreasing ε (and before the creation of new peaks) is different to the one obtained previously $k = 0.82k_{crit}$. Indeed, the coalescence ratio (and consequently

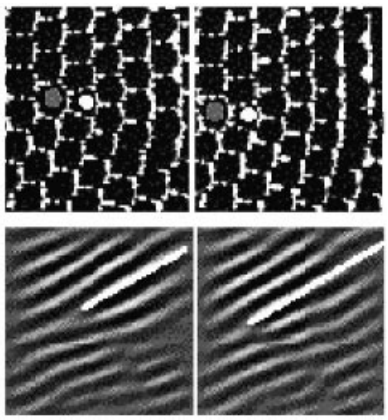

FIGURE 13. Creation of a new peak at a penta–hepta defect: the displacement of the penta–hepta pair along one of the two altered directions can clearly be seen. The images have been filtered and reconstructed in the direction of propagation of the defect. The position of the defect moves along the direction of the brighter white line (lower set of figures).

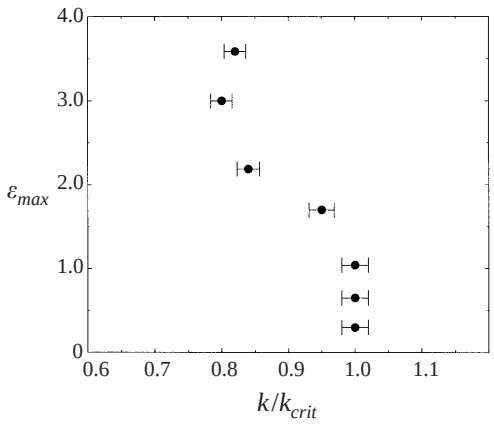

FIGURE 14. Wavenumber of the selected hexagonal pattern on decreasing ε as a function of ε_{max}.

the number of peaks N in the container) depends on the value of ε_{max} (figure 12). When decreasing ε, the hexagonal-pattern wavenumber (before the creation of new peaks) depends on the number of peaks N remaining in the container. We can effect a selection by choosing different values for ε_{max} at any wavenumber $0.82k_{crit} \leqslant k \leqslant k_{crit}$ for the hexagonal pattern, as shown in figure 14. Figure 15 shows a schematic of hysteresis loops as a function of ε_{max} and as a function of the number of peaks in the container.

5.3. *Discussion of the experimental results*

The experimental results of wavenumber selection are discussed in this section. The comparison between the results obtained by the two above processes (quasi-static changes and jumps in magnetic field), indicates that for a magnetic field larger than the critical one, the most stable state is the hexagonal pattern obtained by using jumps in field intensity (figure 11). We deduce that above the onset of instability, both the

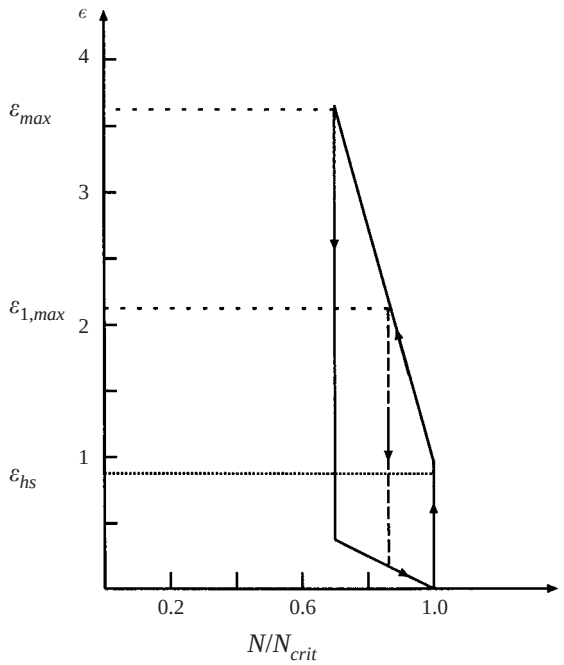

FIGURE 15. Schematic of the selection of the hexagonal pattern wavenumber on decreasing ε, as a function of the number of peaks in the container. ε_{hs} is the hexagon–square transition threshold.

hexagonal pattern at k_{crit} and the square pattern, obtained by the quasi-static process, are metastable states of the system.

Gailitis (1977) studied the relative stability of a hexagonal pattern and a square pattern, both at k_{crit}. He predicted that near the onset of instability, the hexagonal pattern at k_{crit} is the stable state of the system. For higher values of the magnetic field, the hexagonal pattern loses stability in favour of the square pattern, which remains at the k_{crit} during further increase of the magnetic field. From the calculations of Gailitis, it is possible to estimate the stability domains of hexagons and squares as a function of the relative magnetic permeability (μ_r) of the fluid, in the case where $|\mu_r - 1| \ll 1$. Indeed, Herrero *et al.* (1994) have matched the parameters of the Swift–Hohenberg model to the normal field instability. The value of ε_h is defined as the transition threshold from the hexagonal bifurcation branch at $k = k_{crit}$ to the square one, which takes place on increasing the magnetic field. When decreasing the magnetic field, the square bifurcation branch at k_{crit} becomes unstable in favour of the hexagonal branch at k_{crit} for a value of ε denoted ε_s.

The theoretical predictions extrapolated to our ferrofluid, where $\mu_r = 2.4$, indicate that $\varepsilon_s < \varepsilon_h < 0$ is not even in qualitative agreement with our experimental results, $\varepsilon_h = 1.25 \pm 0.18$ and $\varepsilon_s = 1.47 \pm 0.18$, respectively. Our experimental scenario shows the existence of hexagonal and square bifurcation branches at $k \neq k_{crit}$. In the theoretical calculations, only hexagonal and square branches at $k = k_{crit}$ are involved (Gailitis 1977; Herrero *et al.* 1994; Kubstrup *et al.* 1996). These assumptions contradict our experimental results. Hence, we suggest that a more general case should be considered theoretically, allowing for general values of k in order to reach conclusions to be compared with experimental results. We stress again the fact that the amplitude of the surface deformation is large and thus a more nonlinear treatment is probably

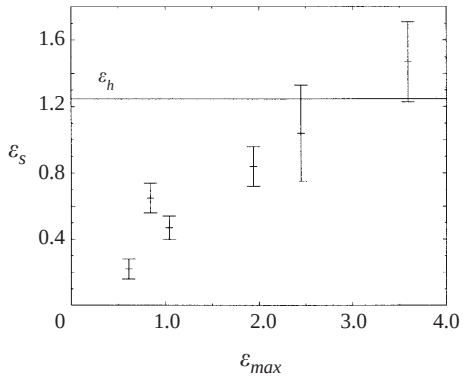

FIGURE 16. Stability onset for the two symmetries ε_s as a function of ε_{max}. We have indicated the experimental value of $\varepsilon_h = 1.25$ with a horizontal line. For small values of ε_{max}, the ε_s value tends qualitatively to the theoretical prediction of $\varepsilon_s \leqslant \varepsilon_h$.

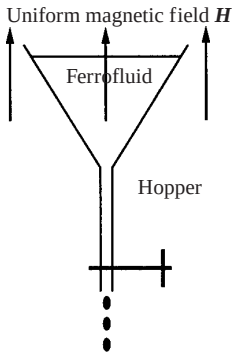

FIGURE 17. Schematic of the compression experiment: a ferrofluid layer under a normal magnetic field $\boldsymbol{H}$, in a hopper; the magnetic field is smaller than for the onset of the hexagon–square transition and remains constant during the experiment.

unavoidable. Furthermore, the theoretical restriction on μ_r does not hold in our experiments.

In order to try to approach the theoretical hypothesis for k, ε_s measurements for various rates of peak coalescences were undertaken. The lower the coalescence rate (i.e. the lower ε_{max}), the more closely the theoretical hypothesis is approached (patterns at k_{crit}). The results are shown in figure 16 and we observe that the theoretical result with $\varepsilon_s \leqslant \varepsilon_h$ becomes more realistic. From a theoretical point of view, Silber & Knobloch (1988) discuss the relative stability of patterns for larger values of μ. However, they could not reach definite conclusions regarding the predicted experimental results.

6. The hexagon–square transition induced directly by compression

6.1. *Experimental set-up*

Experiments were performed where the transition is induced by isotropic compression of the hexagonal pattern. The experimental design is sketched in figure 17. A ferrofluid layer, in a hopper, is subjected to a vertical magnetic field, produced by the Helmholtz coils described in § 2. The magnetic field is increased continuously from zero to a

certain field strength, which is smaller than for the onset of the hexagon–square transition $\varepsilon_{hs} = 0.84 \pm 0.17$. As a consequence, a hexagonal pattern is established in the hopper. We check that its wavenumber corresponds to the capillary one k_c (within an experimental error of 3%), as seen in § 5.2. Due to the system geometry (and in particular due to the boundary conditions in the hopper) the magnetic field is uniform to within 10% over the ferrofluid surface. In order to compress the hexagonal pattern, the hopper is opened and the ferrofluid flows out drop-by-drop. This quasi-static process produced very little hydrodynamic disturbance at the surface. The magnetic field varied less than 5% during the whole experiment, and this was due to the variable ferrofluid layer thickness.

A selection from a sequence of photographs taken every 4.5 minutes, during a typical experiment performed at $\varepsilon = 0.75 \pm 0.19$, is shown in figure 18. The upper diameter is reduced by 2% in each picture, and corresponds to a wavenumber variation of 2% (when the number of peaks remains a constant). Figure 18 shows that the hexagonal pattern transforms continuously into a square pattern. At a rate of compression of 7%, the initial hexagonal pattern clearly exhibits elements of square symmetry (figure 18, picture 7). The variation in the number of peaks during the experiment, as a function of the upper diameter reduction, is displayed in figure 19: the transformation occurs first at fixed number of peaks, until picture 9 in figure 18. In picture 13, the square pattern is clearly established in the container. When too many peaks disappear (pictures 17 and 19), the compression rate of the hexagonal pattern decreases and the square symmetry loses stability in favour of triangular symmetry.

The quantitative results of compression in figure 20 show the onsets of transition after compressing the hexagonal pattern at k_c (◆), for different values of ε ($< \varepsilon_{hs}$). Also shown are the transition onsets after compressing the hexagonal pattern down to about 5% of the original size, for different constant values of ε, and then increasing ε (◇). It transpires that we can induce the transition by two procedures: either directly by increasing the magnetic field, or by compressing the hexagonal pattern. The exploration of the stability domain of a given configuration in the hopper is limited for various reasons. First, the accessible range of the elastic compression is narrow (about 10% of k_c), and the measurement precision of the compression rate is low. Secondly, the accessible range of ε is small as it satisfies $\varepsilon < \varepsilon_{hs}$. Increasing the magnetic field and compressing the hexagonal pattern appear to be two equivalent procedures that induce the transition. They both allow the magnetic coupling between peaks to be increased.

6.2. *Discussion of the results of compression*

The next consideration is the reason for the appearance of the square pattern. On varying ε in a quasi-static way, the hexagonal pattern develops at k_{crit} and its wavenumber remains constant for increasing values of ε. Moreover, at the transition the number of peaks remains constant. This observation suggests that the boundary conditions (such as the existence of a meniscus at the lateral walls) do not allow the system to reach a stable state by decreasing its wavenumber. Clearly, the boundary conditions, and presumably the nonlinearities induced by the large amplitude of the peaks, gives a metastable character to a number of configurations at a fixed field. This is supported by the hysteretic behaviour discussed earlier with respect to field variation. Hence, in this picture, the stability is due to the 'high energetic cost' of creation or loss of a new peak. The hopper experiment allows this stability to be probed by inducing a strain on the pattern of peaks, i.e. changing the wavenumber at a fixed number of peaks. When the hopper is emptied, the elastic compression first induces a hexagonal to square transition comparable to the one observed on increasing

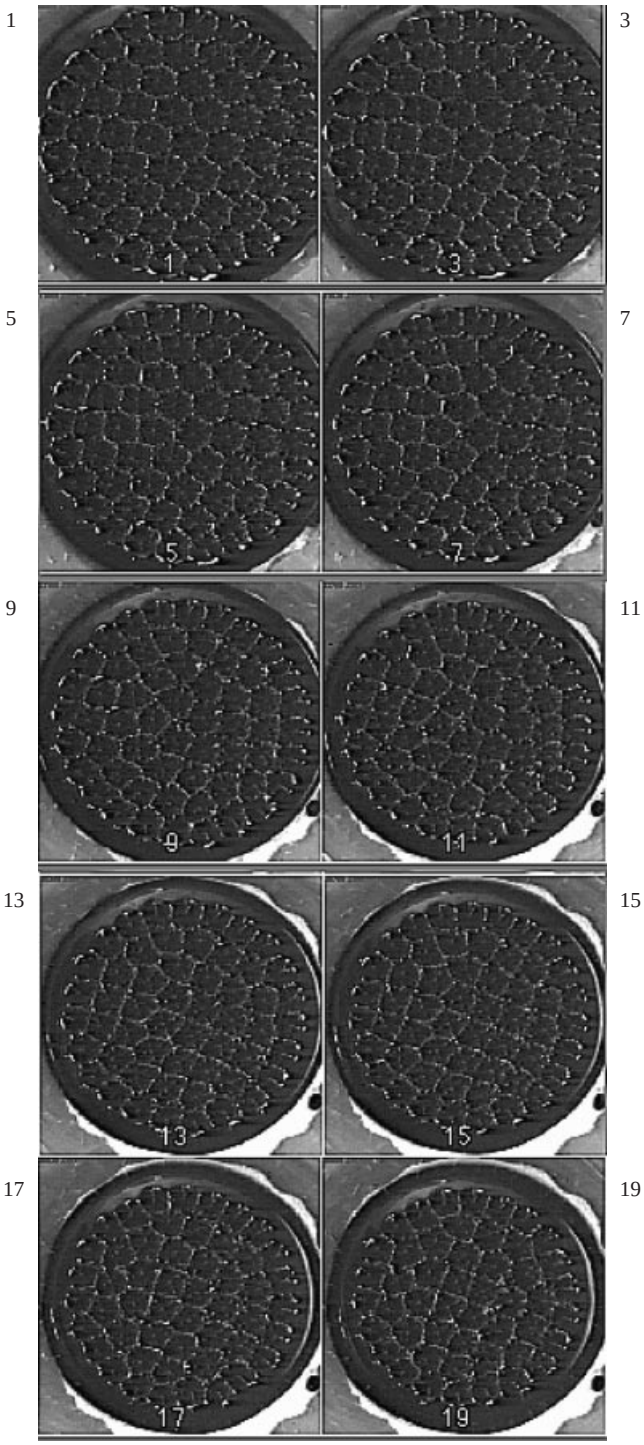

FIGURE 18. When the hexagonal pattern is compressed in the hopper, the transition to the square pattern is observed. The square symmetry reorganizes into triangular symmetry commencing from picture 17 through the disappearance of peaks within the pattern and as a consequence, reduces the compressive stress. These photographs were taken 9 minutes apart.

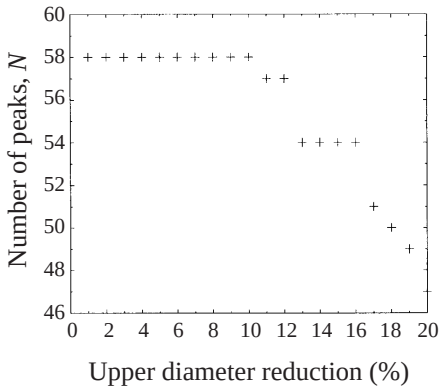

FIGURE 19. Compression of the hexagonal pattern: number of peaks in the container as a function of the upper diameter variation.

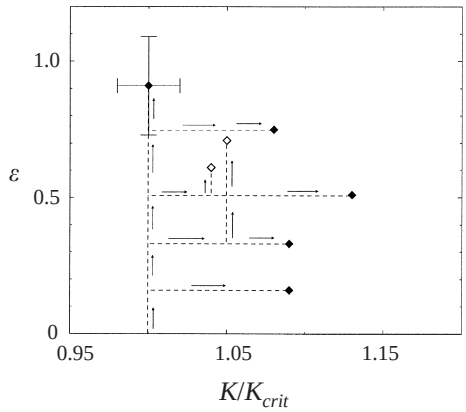

FIGURE 20. Transition onset: ◆, by compressing the hexagonal pattern at k_c at constant ε; ◇, by compressing down to 5% the hexagonal pattern at k_c at constant ε and then increasing ε. The dotted lines represent the paths taken by the system to equilibrium.

the field. This novel experiment allows us to independently vary k and ε, and then explore the domain of stability of a given configuration. A further development of this experiment would be to analyse it in terms of phase dynamics (Brand & Wesfreid 1989; Lauzeral, Metens & Walgraef 1993).

7. Conclusion

We have studied experimentally the hexagon–square transition. Sufficiently far from the threshold of the primary instability, the hexagonal pattern loses stability in favour of the square pattern. The transition is triggered by penta–hepta defects, present in the hexagonal pattern. We show that the square pattern is first formed at the core of the defect, from the non-altered mode in the hexagonal pattern. In the experiments, the onset of the morphological transition occurs at $\varepsilon_{hs} = 0.84 \pm 0.17$ when there are penta–hepta defects and at $\varepsilon_{hs} = 1.04 \pm 0.17$ otherwise. We describe the phenomenology of the transition. This begins when one row of peaks translates along its orientation axis. This motion locally transforms the triangular symmetry into a strained square symmetry. The mechanism of the transition implies a change in wavenumber at the onset because the number of peaks remains constant, a result which has not been taken

into account in theoretical calculations. Moreover, we observe stable fronts between the two symmetries, where the perpendicular wavevector to the front is conserved. We focus our interest on pattern and wavenumber selection, by varying both the magnetic field in a quasi-static way and using jumps in field intensity. On varying the magnetic field in a quasi-static manner, the hexagon–square transition with an hysteresis loop is observed. These are qualitative and quantitative differences with the theoretical results for the onsets of the stability domains of the hexagons and squares. These differences are interpreted as the result of restrictive conditions considered in theoretical models, such as the assumption that the patterns remain at k_{crit} on increasing and decreasing ε, and the assumption that $|\mu_r - 1| \ll 1$. These assumptions are not generically valid in experiments. On using jumps in field intensity from an initially flat interface, the hexagonal pattern is always favoured. The larger the magnetic field, the smaller the wavenumber. A comparison between the results for wavenumber selection obtained by the two processes leads us to conclude that the square pattern is a metastable state induced by compression of the hexagonal pattern. To confirm this, we have performed a new experiment, in a hopper, where we induce the transition by directly compressing the hexagonal pattern at constant magnetic field.

We are grateful to S. Krishnamurthy, J.-B. Manneville and C. Pérez-Garcìa for very fruitful discussions.

REFERENCES

Abou, B. 1998 Instabilité de pics dans les ferrofluides; étude de la transition hexagones-carrés. PhD thesis, University Paris VI, France.

Abou, B., Néron de Surgy, G. & Wesfreid, J.-E. 1997 Dispersion relation in a ferrofluid layer of any thickness and viscosity. *J. Phys.* II (*Paris*) **7**, 1159.

Allais, D. & Wesfreid, J.-E. 1985 Instabilité de surface dans les ferrofluides. *Bull. Soc. Fr. Phys. Suppl.* **57**, 20.

Bacri, J.-C., Perzynski, R. & Salin, D. 1988 Instabilité d'un film de ferrofluide. *C. R. Acad. Sci. Paris* **307**, 699.

Bestehorn, M. 1996 Square patterns in Bénard–Marangoni convection. *Phys. Rev. Lett.* **76**, 46.

Boudouvis, A. G., Puchalla, J. L., Scriven, L. E. & Rosensweig, R. E. 1987 Normal field instability and patterns in pools of ferrofluid. *J. Magn. Mat.* **65**, 307.

Bragard, J. & Velarde, M. G. 1998 Bénard–Marangoni convection: planforms and related theoretical predictions. *J. Fluid Mech.* **368**, 165.

Brancher, J.-P. 1980 Interfacial instability in viscous ferrofluids. *IEEE Trans. Magn.* **MAG-16**, 1331.

Brand, H. & Wesfreid J.-E. 1989 Phase dynamics for pattern equilibrium systems under an external constraint. *Phys. Rev.* A **39**, 6319.

Ciliberto, S., Coullet, P., Lega, J., Pampaloni, E., & Pérez-Garcìa, C. 1990 Defects in roll-hexagon competition. *Phys. Rev. Lett.* **65**, 2370.

Ciliberto, S., Pampaloni, E., & Pérez-Garcìa, C. 1991 The role of defects in the transition between different symmetries in convective patterns. *J. Statist. Phys.* **64**, 1045.

Coullet, P., Emilson, K. P. & Plaza, F. 1991 Qualitative theory of defects in non-equilibrium systems. In *Instabilities and Nonequilibrium Structures* (ed. E. Tirapegui & W. Zeller), vol. III. Kluwer.

Cowley, M. D. & Rosensweig, R. E. 1967 The interfacial stability of a ferromagnetic fluid. *J. Fluid Mech.* **30**, 671.

Gailitis, A. 1977 Formation of the hexagonal pattern on the surface of a ferromagnetic fluid in an applied magnetic field. *J. Fluid Mech.* **82**, 401.

Herrero, H., Pérez-Garcìa, C. & Bestehorn, M. 1994 Stability of fronts separating domains with different symmetries in hydrodynamical instabilities. *Chaos* **4**, 15.

KUBSTRUP, C., HERRERO, H. & PÉREZ-GARCÌA, C. 1996 Fronts between hexagons and squares in a generalized Swift–Hohenberg equation. *Phys. Rev.* E **54**, 1560.

KUZNETSOV, E. A. & SPEKTOR, M. D. 1976 Existence of a hexagonal relief on the surface of a dielectric fluid in an external electrical field. *Sov. Phys. JETP* **44**, 136.

LAUZERAL, J., METENS, S. & WALGRAEF, D. 1993 On the phase dynamics of hexagonal patterns. *Europhys. Lett.* **24**, 707.

MELO, F., UMBANHOWAR, P. B. & SWINNEY, H. 1995 Hexagons, kinks, and disorder in oscillated granular media. *Phys. Rev. Lett.* **75**, 3838.

NITSCHKE-ECKERT, K. & THESS, A. 1995 Secondary instability in surface-tension-driven Bénard convection. *Phys. Rev.* E **52**, R5772.

PANTALONI, J. & CERISIER, C. 1983 Structure defects in Bénard–Marangoni instability. In *Cellular Structures in Instabilities* (ed. J. E. Wesfreid & S. Zaleski). Lecture Notes in Physics, vol. 210, p. 197. Springer.

RIBOTTA, R. & JOETS, A. 1983 Defects and interactions with the structures in ehd convection in nematic liquid crystals. In *Cellular Structures in Instabilities* (ed. J. E. Wesfreid & S. Zaleski). Lecture Notes in Physics, vol. 210, p. 249. Springer.

ROSENSWEIG, R. E. 1985 *Ferrohydrodynamics*. Cambridge University Press.

SALIN, D. 1993 Wave vector selection in the instability of an interface in a magnetic or electric field. *Europhys. Lett.* **21**, 667.

SCHATZ, M., VANHOOK, S. J., MCCORMICK, W. D., SWIFT, J. B. & SWINNEY H. L. 1999 Time-independent square patterns in surface-tension-driven Bénard convection. *Phys. Fluids* **11**, 2577.

SILBER, M. & KNOBLOCH, E. 1988 Pattern selection in ferrofluids. *Physica* D **30**, 83.

TWOMBLY, E. & THOMAS, J. W. 1980 Mathematical theory of non-linear waves on the surface of a magnetic fluid. *IEEE Trans. Magn.* **MAG-16**, 214.

VALET, T. & WESFREID, J.-E. 1988 Experiments and an improved model of the instabilities of thin viscous layers of magnetic liquids. In *Dispersive Waves in Dissipative Fluids* (ed. D. G. Crighton & F. Mainardi), p. 62. Bologna, Italy. Alma Mater Studiorum.

WESFREID, J.-E. & ZALESKI S. 1983 (Eds.) *Cellular Structures in Instabilities*. Lecture Notes in Physics, vol. 210. Springer.

ZELAZO, R. E. & MELCHER, J. R. 1969 Dynamics and stability of ferrofluids: surface interactions. *J. Fluid Mech.* **39**, 1.